Earth and Planetary Science Letters 275 (2008) 308–319

Contents lists available at ScienceDirect

Earth and Planetary Science Letters

journal homepage: www.elsevier.com/locate/epsl

Paleomagnetism of Lonar impact crater, India

Karin L. Louzada [a,*], Benjamin P. Weiss [b], Adam C. Maloof [c], Sarah T. Stewart [a], Nicholas L. Swanson-Hysell [c], S. Adam Soule [d]

[a] Department of Earth and Planetary Sciences, Harvard University, 20 Oxford Street, Cambridge, MA 02138, USA
[b] Department of Earth, Atmospheric and Planetary Sciences, Massachusetts Institute of Technology 54-814, 77 Massachusetts Avenue, Cambridge, MA 02139, USA
[c] Department of Geosciences, Guyot Hall, Princeton University, Princeton, NJ 08544, USA
[d] Woods Hole Oceanographic Institution, Clark S 272C, MS#24, Woods Hole, MA 02540, USA

ARTICLE INFO

Article history:
Received 9 January 2008
Received in revised form 5 August 2008
Accepted 19 August 2008
Available online 2 October 2008

Editor: T. Spohn

Keywords:
Lonar
impact
crater
shock
paleomagnetism
remanent magnetization

ABSTRACT

Lonar crater, India, is the best preserved terrestrial impact crater formed in basalt and is a unique terrestrial analogue for small, simple craters on terrestrial planets and the Moon. We investigated the paleomagnetic and rock-magnetic properties of the 1.88 km diameter crater in order to understand the effect of impacts on magnetization in target rocks. The magnetization in the Lonar basalts consists of an original 65 Ma Deccan magnetization and a recent overprint. We constrained the timing of magnetization acquisition at Lonar using a combination of conglomerate tests on ejecta deposit clasts and fold tests on the overturned and jumbled rim fold. In some areas, the recumbent rim fold is preserved and can be approximated as a horizontal cylindrical fold. In other areas, substantial vertical axis rotation may have occurred where tear zones developed during folding. We observed only subtle effects from the impact on the rock-magnetic properties of Lonar materials, which include a slightly elevated coercivity in shocked ejecta blocks. We show that paleomagnetism can provide a constraint on shock heating in the absence of petrographic evidence of shock (in this case, $<187 \pm 15$ °C). At Lonar, viscous (and/or chemical) remanent magnetization acquired in the <50 kyr subsequent to crater formation has obscured any evidence of shock remanent magnetization. We also find no evidence of shock demagnetization or the presence of intense impact-induced or impact-amplified transient magnetic fields that have been proposed around larger impact structures.

© 2008 Elsevier B.V. All rights reserved.

1. Introduction

Remanent magnetization is present in many extraterrestrial materials. It is desirable to utilize the magnetism of meteorites, asteroids and planetary surfaces in order to interpret the magnetic history of their parent bodies. Because impacts are ubiquitous throughout the solar system, nearly all of these materials have been modified to a certain degree by shock(s). Thus, an understanding of the magnetic effects of shock on rocks is crucial. Low pressure shock demagnetization may have led to unmagnetized regions around impact basins on Mars (Hood et al., 2003). Remagnetization of surface materials through impact-generated plasma fields is thought to have occurred at the ~300 km diameter Vredefort impact structure, South Africa (Carporzen et al., 2005) and in the lunar crust (Lin et al., 1998). The magnetic properties of shocked meteorites, and rocks and minerals under pressure, are more frequently being used to interpret the composition of the Martian crust (Kletetschka et al., 2004; Bezaeva et al., 2007).

Lonar crater, India, provides an unparalleled opportunity to study naturally shocked basalts in a geologically simple setting on Earth. Lonar is located at 19°58′ N, 76°31′ E in the Deccan flood basalt province. As the youngest, freshest and best-exposed terrestrial impact crater formed in basalt, it is an excellent analogue for small, simple craters on other planetary bodies. Lonar is assumed to have formed <50 ka (Fredriksson et al., 1973a; Sengupta et al., 1997), and possibly <12 ka (Maloof et al., in press). The simple, bowl-shaped crater has a present-day average rim to rim diameter of 1.88 km and average rim height of 30 m (Maloof et al., in press). The crater is approximately 150 m deep (from the rim) with a shallow saline lake at its bottom (depth to water level is 137 m). The crater's origin was debated for many years (Gilbert, 1896; La Touche and Christie, 1912; Lafond and Dietz, 1964; Pal and Ramana, 1972; Crawford, 1983; Subrahmanyam, 1985), until its impact origin was confirmed by the discovery of shocked materials such as shatter cones, maskelynite and impact glasses (Fredriksson et al., 1973a; Murali et al., 1987; Nayak, 1972, 1993).

At Lonar, five to six, 5 to 40-m thick, tholeiitic basalt flows are exposed in the crater walls. Massive fine-grained basalt flows typical of the Deccan plateau grade upwards into vesicular flow tops which may contain up to 20 vol.% vesicles 1 to 20 mm in diameter (e.g. Kieffer et al., 1976). The flows in the crater walls are upturned, dipping 10 to 20° radially outwards (Fudali et al., 1980; Kumar, 2005). Near the rim crest the dips are steeper and commonly vertical or overturned at the rim fold. One layer parallel slip fault is observed near the spring at Dhar Canyon

* Corresponding author. Tel.: +1 617 495 8986; fax: +1 617 495 0635.
E-mail address: louzada@fas.harvard.edu (K.L. Louzada).

0012-821X/$ – see front matter © 2008 Elsevier B.V. All rights reserved.
doi:10.1016/j.epsl.2008.08.025

(Fig. 1). The extent of the original continuous ejecta blanket has been reduced (from 2.5 crater radii, Rc; Fudali et al., 1980) due to expansion of the town and agriculture in the south and southwest.

We conducted a paleomagnetic study of oriented rocks from Lonar crater to: 1) test the hypothesis of shock remanent magnetization at Lonar (Poornachandra Rao and Bhalla, 1984), 2) find evidence of impact-amplified and/or impact-generated magnetic fields (Srnka et al., 1979; Crawford and Shultz, 1988), and 3) identify potential magnetic shock indicators (Cisowski and Fuller, 1978).

2. Setting the scene

2.1. The Lonar impact event

To interpret the paleomagnetism of Lonar crater within the context of impact cratering, we first set out the events that took place during crater formation (see also Melosh, 1989). The impact conditions for Lonar are not known; no magnetic meteorite fragments or localized enrichments of metals have been observed (Venkatesh, 1967; Stroube et al., 1978; Son and Koeberl, 2007).

During the contact and compression stage, a rocky asteroid (roughly 55 m in diameter) or icy comet (roughly 40 m in diameter) struck the surface at 20 or 50 km/s respectively (based on crater scaling, Melosh and Beyer, 1998). In about 10^{-2} seconds, a strong shock wave compressed the projectile and target material causing both to melt or vaporize (shock pressures of 10^2 GPa) in a region of radius approximately 1.6 times the projectile radius (Pierazzo et al., 1997). Release of the shock state by rarefaction waves from the free surface initiated the excavation stage. In less than 0.2 second, the hemispherical shock wave had become detached and propagated roughly 1 km into the target, compressing and accelerating the material it travelled through. After approximately 6 seconds (Melosh and Beyer, 1998), an outward excavation flow had opened a hemispherical crater many times larger than the projectile. Formation of the ejecta curtain and expansion of a vapor plume were also initiated at this time. Ejecta emplacement however, did not come to an end until minutes later, well after the crater cavity formed. The last materials to be deposited were the shock-melted and recondensed materials, such as spherules.

During the modification stage, the transient hemispherical cavity collapsed slightly under gravity when loose debris slumped down the crater walls to create a bowl-shaped crater approximately 1710–1780 m in diameter (Fudali et al., 1980; Maloof et al., in press).

Subsequent erosion has resulted in a further widening of the crater and reduction of the crater rim height.

2.2. Acquisition of magnetization

During initial emplacement and cooling of the basalt flows 65.5 Ma, the basalts would have acquired a primary magnetization when the magnetic field was reversely oriented (chron C29R; at Lonar Declination

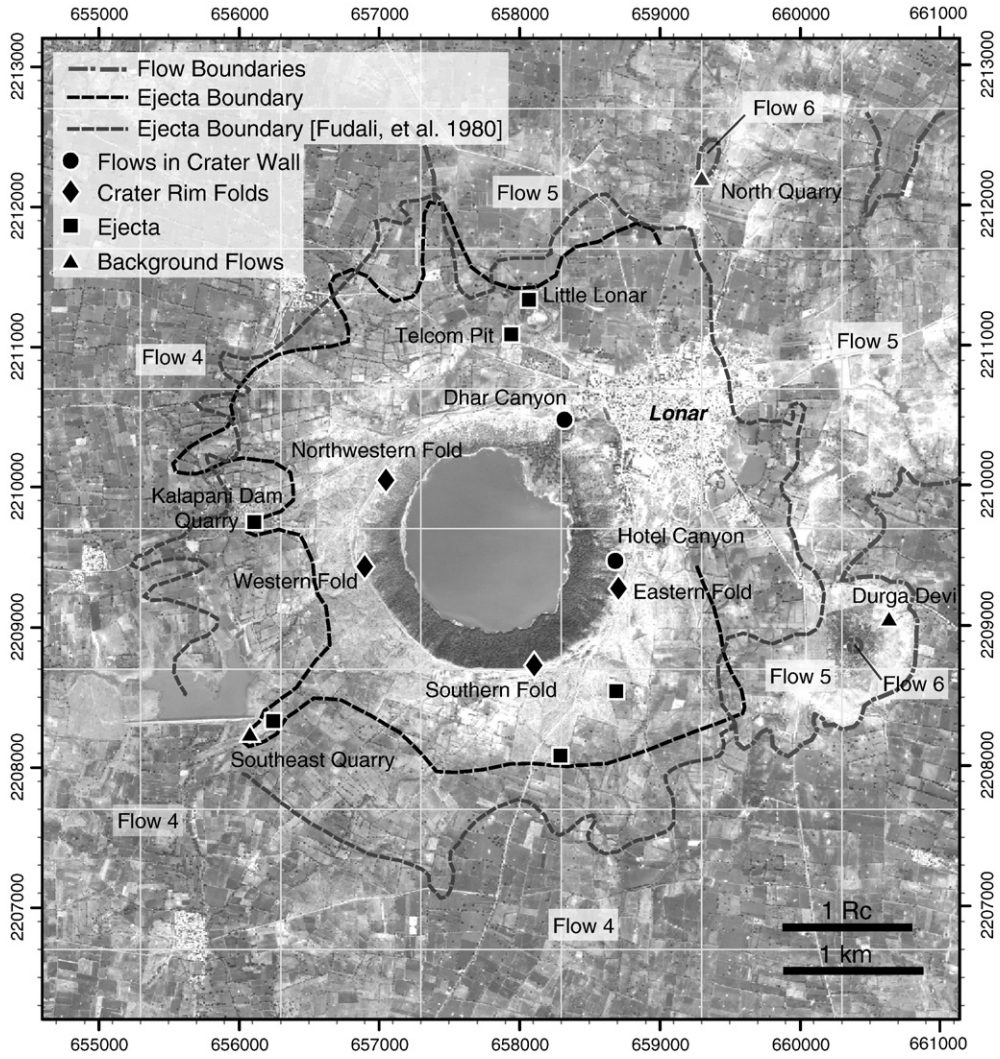

Fig. 1. Quickbird image of Lonar crater showing the locations of the paleomagnetic sampling sites. See Table 1S for GPS locations of the paleomagnetic sites (UTM, WGS 84). An additional site is located to the south east of the crater at Pimpalner Dam (at 8.1 Rc), where there is an outcrop of unshocked background flow 4. Rc denotes crater radius (0.94 km).

(Dec.)=157.6°, Inclination (Incl.)=+47.4°, α_{95}=1.9°; Vandamme et al., 1991; Courtillot et al., 2000). Approximately 50 ka, just prior to the impact, the magnetic field was normally directed as it is today (Dec.=−0.8°, Incl.=28.0°, IGRF, 2007; with (α_{95}=) 8.8° secular variation for the past 10 kyr, Elmaleh et al., 2004). and the Lonar basalts would have acquired a secondary viscous remanent magnetic (VRM) overprint parallel to the present-day local geomagnetic field (hereafter PLF). At the time of impact, a new shock remanent magnetization (SRM) could have been acquired during the brief period of shock compression in the presence of an impact-generated or the ambient geomagnetic field (e.g., Nagata, 1971; Srnka et al., 1979; Gattacceca et al., 2007a). The timing and location of acquisition of SRM control the resultant intensity and direction.

Spontaneous impact-generated magnetic fields have been produced in laboratory experiments during the contact and compression stage (Srnka et al., 1979; Crawford and Schultz, 1991, 1993, 1999). In the presence of an ambient magnetic field, inward directed flow of the plasma cloud during cavitation behind the projectile can lead to a brief enhancement of the ambient magnetic field within 1 to 3 projectile radii, largely where the shock has led to melting or vaporization.

The impact-generated plasma then expands freely leading to rapid decay of the field, so that most of the crater excavation and ejecta emplacement take place after the peak impact-generated fields have decayed away.

We expect SRM to be nonunidirectional for two reasons. Impact generated magnetic fields in laboratory experiments generally exhibit significant bilateral anti-symmetry in both magnetic intensity and polarity, varying with spatial wavelengths on the order of crater-radii (see e.g., Fig. 3 in Crawford and Schultz, 1993). We expect this spatial complexity of the magnetic field to be reflected in the directionality of SRM acquired during the brief period of compression, in both the ejecta clasts and in situ bedrock samples (Fig. 2e and f). Rim blocks and ejecta blocks thrown out of the crater would have acquired SRM prior to folding and ejection, and would have been further randomized as a result of translation and rotation during folding and deposition.

Therefore, even if SRM was acquired in the presence of the ambient geomagnetic field, we would not expect the observed SRM to be unidirectional (Fig. 2c and d). After the formation of the crater, and the decay of any impact-generated fields, the rocks would have continued to viscously acquire magnetization parallel to the PLF in their final locations and orientations (Fig. 2g and h).

Considering the sequence of events outlined above, we define the following paleomagnetic test to rule out SRM (Fig. 2): a negative conglomerate test result (or randomness; Watson, 1956) on both the ejecta and the folded rim, and failure of the fold test (McElhinny, 1964) by default. Both post-impact VRM (Fig. 2g) and heterogeneous SRM (Fig. 2e) will fail a fold test; the former will do so because it is unidirectional, and the latter because it was acquired randomly.

2.3. Numerical model results

To estimate the peak shock pressure and temperature fields at Lonar, we conducted a numerical simulation (Fig. 3) of the impact using the shock physics code CTH (McGlaun et al., 1990) with the ROCK strength model (Senft and Stewart, 2007). In order to produce a Lonar-sized final (pre-erosion) crater in CTH, we modeled a 70 m diameter projectile, with uncompressed density of 2900 kg/m^3 (equal to the fresh, dense target basalt, Fudali et al., 1980), travelling at 20 km/s. Although the impact was unlikely to be vertical, modeling it as such reduces the numerical problem to 2D with cylindrical symmetry, with minimal effect on the results for this work.

The modeled crater, about 30 s after impact (Fig. 3) has a breccia lens in the bottom of the crater, upturned beds in the crater wall and an overturned fold at the crater rim (Fig. 3c). The predicted breccia lens is approximately 180 m thick, whereas drill cores at Lonar have shown it to be at least 225 m (Fredriksson et al., 1973a; see also Grieve et al., 1989). This 20% difference in thickness could be explained by the increase in porosity of the breccia, which was not accounted for in the simulation. Presently, approximately 100 m of lake sediment and 6 m of water overly the breccia lens. The present topography is a result of the subsequent erosion of the crater walls and the presence of a lake.

The shock intensities expected at Lonar are modest (Fig. 3a and b). Shocked materials, with pressures greater than the Hugoniot elastic

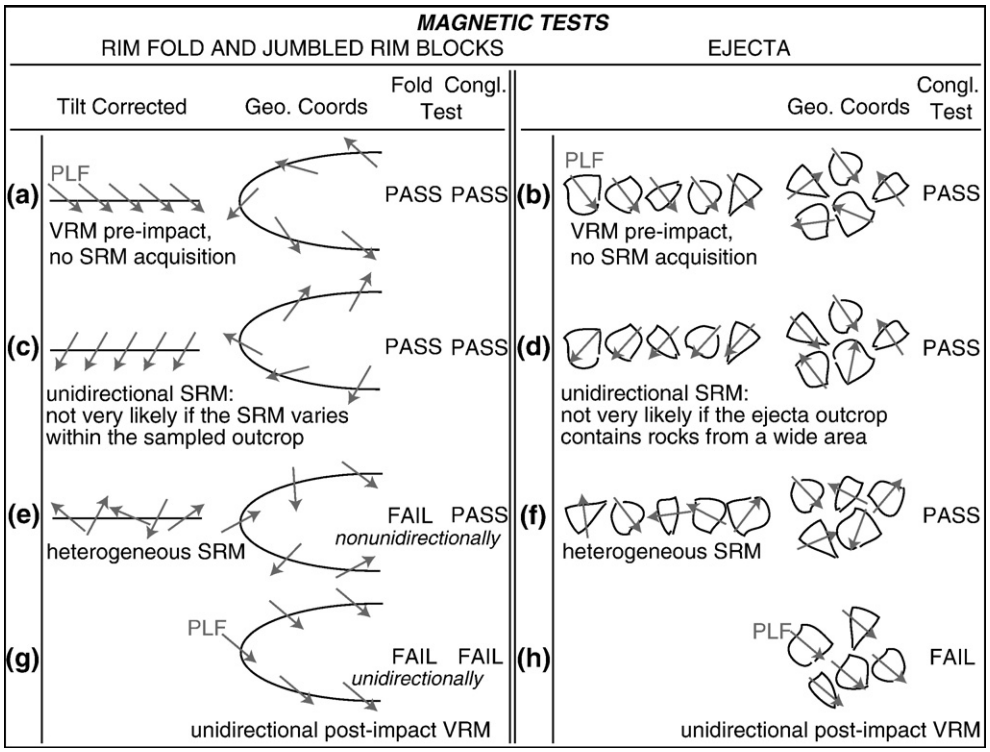

Fig. 2. Schematic drawing showing directional magnetic tests for the determination of the origin of the magnetic remanence in rim fold and ejecta rocks. Geo. Coords=geographic coordinates; Congl. Test=conglomerate (randomness) test; Tilt Corrected=prefolding/unfolded orientation.

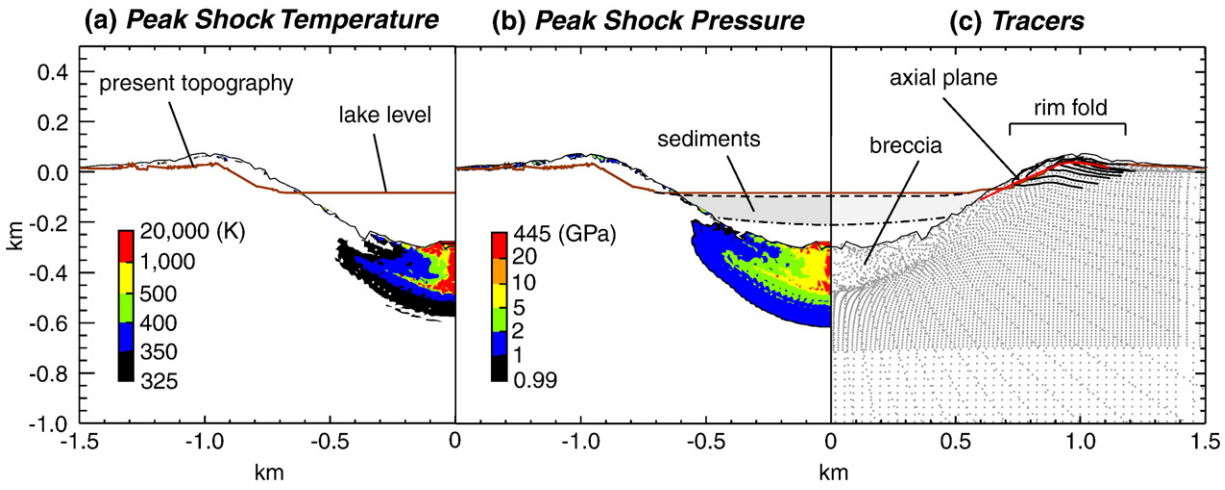

Fig. 3. Numerical simulation (shock physics code CTH) results ~30 s after impact of a 70 m diameter basalt projectile into basalt at 20 km/s. Peak shock temperature (a) and pressure (b) achieved during the simulation. (c) Final locations of tracers in initially horizontal beds and radial arrays. The current water depth of the lake is ~6 m (dashed line) and ~100 m of lake sediment overlies the breccia lens (the dash–dotted line is a sketch of the lowest extent of the lake sediment). Down warping of the rim fold (a curved axial fold plane) is a result of slumping of the crater walls during the modification stage of crater formation. Subsequent erosion of the crater walls has further reduced the height of the crater rim and opened up the crater. Color version available online.

limit of basalt (~5 GPa; Nakazawa et al., 1997), and temperatures above 200 °C, are restricted to the thick breccia lens directly below the crater floor and a small fraction of the ejected volume. Estimated shock pressures of ejecta clasts based on petrographic studies are up to 60 GPa and the bulk of the ejecta shows no evidence of shock due to low shock pressures and the entrainment of unshocked clasts from the surrounding surface in the ejecta debris flow (Fredriksson et al., 1973a; Fudali et al., 1980). The numerical estimates agree well with these observations and experimentally shocked Lonar basalt (Kieffer et al., 1976). Deccan flows sampled at distances greater than 2.4 Rc suffered only elastic deformation and are considered to be unshocked background flows. Due to the zero pressure boundary condition at the surface, the upper parts of the crater walls and the crater rim folds in the interference zone suffered low pressures as well (<5 GPa). Only a thin veneer of moderately shocked material coated the pristine crater. In addition, scattered spherules were found in the upper most layer of the ejecta blanket (Nayak, 1972; Fredriksson et al., 1973b; Maloof et al., in press). Many previous magnetic studies of craters have focused on intensely shocked materials at larger impact structures such as Vredefort, South Africa (~300 km original diameter, Hart et al., 1995; Carporzen et al., 2005), Sudbury, Canada (250 km, Szabó and Halls, 2006) and Chixculub, Mexico (170 km diameter, Urrutia-Fucugauchi et al., 2004) where heating was extensive and resulted in the development of melt sheets. In this study, we compare rocks from the crater rim and surrounding ejecta blanket, to unshocked background basalts, to search for the effects of low to moderate shock on the paleomagnetic and rock-magnetic signatures in the rocks.

3. Methods

During two field seasons (2005 and 2006), 270 oriented core and block samples were collected from 16 sites in and around the crater (Fig. 1, Table 1S) subdivided into four groups:

I. flows in the upper crater wall, below the hinge of the overturned flap (two sites),
II. recumbently folded and brecciated flows at the crater rim (four sites),
III. ejecta (six sites between 1.4 and 2.2 Rc), and
IV. unshocked flows (four sites between 2.4 and 8.0 Rc from the crater center).

Where possible, bedding was identified using flow banding on the scale of meter-sized blocks or vesicle-abundance contrasts on the scale of 10 to 100-m outcrops. All magnetic measurements were corrected for the site mean declination of the PLF. Approximately 30 samples were removed from the dataset because of the suspicion that they had been remagnetized by lightning for the following reasons: the measured declination of the local magnetic field deviated more than 10° from the PLF, their magnetization was near saturation and single component, or they had random demagnetization trends. The majority of these samples were from lightning prone sites at topographic highs: along the crater rim (38%) and upper part of the crater wall (35%). It is unlikely that these samples were exposed to the most intense impact-related magnetic fields or that they were shocked substantially (Fig. 3, Section 2.3).

Four sets of experiments were conducted. The goal of the first set of experiments ('AF+TH') was to measure the natural remanent magnetization (NRM) of the samples. Specimens approximately 1 cm thick were cut from 2.5 cm diameter cores from all sites. The specimens were subjected to: (i) measurement of NRM, (ii) immersion in liquid nitrogen for removal of magnetization carried by multidomain hematite and magnetite, (iii) step-wise alternating-field (AF) demagnetization in three directions in 2 mT steps up to 10 mT, and (iv) step-wise thermal demagnetization in 30 steps from 50 to 680 °C with decreasing step size from 50 to 20°C.

The goal of the second and third experiments was to study the effects of shock on the magnetic remanence and magnetic properties of the basalts. In the second experiment ('TH only') two or three additional specimens from each site were subjected only to thermal demagnetization from 50 to 250 °C in 10 °C steps (without submersion in liquid nitrogen and AF demagnetization). In the third experiment ('Rockmag') 21 chips of representative specimens, with masses ranging between 13 and 382 mg, were subjected to rock-magnetic measurements of coercivity (magnetic hardness) of NRM and saturation isothermal remanence (SIRM, at ~1 T) through AF demagnetization up to 85 mT in 22 steps with increasing step size from 2.1 to 6.1 mT.

In the fourth experiment ('VRMacq') seven specimens were placed in a 47 μT field and allowed to acquire a viscous remanent magnetization which was measured at first every few minutes and later once a day. The direction of the ambient field was measured using a three-axis portable MEDA Inc. fluxgate magnetometer with 1 nT sensitivity, and made an angle of 11 to 118 degrees with the NRM in the specimens. After 9 to 16 days, two specimens were placed in a magnetically shielded room (<150 nT) and their VRM was allowed to decay.

All paleomagnetic and rock-magnetic measurements were conducted using 2G Enterprises Super-conducting Rock-magnetometers, equipped with automated sample changers, at the Paleomagnetism Laboratories of

the California Institute of Technology and the Massachusetts Institute of Technology. The sensitivity limit of the magnetometers was 10^{-12} Am^2, well below the average range of individual sample measurements (10^{-8}–10^{-5} Am^2). Stepwise heating was conducted in a magnetically shielded furnace in a nitrogen-rich atmosphere to minimize oxidation. Magnetic components revealed by stepwise demagnetization were identified using principal component analysis (Kirschvink, 1980).

4. Paleomagnetism of Lonar crater

4.1. Lonar magnetic mineralogy

Previous studies at Lonar found the basalts consist of 10 to 20 vol.% iron-titanium oxides, most of which are nonmagnetic ilmenite and ülvospinel (Schaal, 1976). Micron-size Ti-rich exsolution lamellae divide ferromagnetic Ti-poor titanomagnetite grains (tens of microns in size) into interacting single-domain needles of high coercivity; although some grains have poorly developed lamellae and low coercivities (Evans and Wayman, 1974; Cisowski and Fuller, 1978).

Alteration of the oxidized titanomagnetites during heating (in Ar) is exhibited by an increase in susceptibility at ~275 °C in a background basalt (from Pimpalner Dam at ~8.1 Rc; Fig. 1S in the online supplemental material), which prevents an estimation of the titanium content based on the Curie temperature (~580 °C).

4.2. Natural remanent magnetization in the Lonar rocks

Two components of magnetization were identified in nearly all samples in 'AF+TH' experiments, evidenced by a change in direction in orthogonal demagnetization plots (Figs. 4 and 2S; after Zijderveld, 1967). A low-coercivity/low-temperature component, *LC_LT*, was easily removed by AF cleaning and low-temperature step-wise heating (50–200 °C). Continued heating revealed a high-temperature component, *HT*, until the demagnetization trends became erratic, intensity no longer changed and measurement error angles increased. Based on the paleomagnetic test results set out in Section 2.2 (Fig. 2), and comparisons with the paleo-Deccan direction and PLF (Table 2S), we interpret these components as either 1) primary, 2) shock remanent or, 3) post-impact magnetization.

4.2.1. Background flows and flows exposed in the crater walls

The mean *LC_LT* (in geographic coordinates) in each of the four flows is roughly parallel to the PLF (Fig. 5). Averaged over all flows, *LC_LT* (D=7.4°, I=+30.7°, α_{95}=5.5°) is statistically identical to the PLF with 95% confidence.

HT directions are approximately reversed with respect to *LC_LT* and are statistically identical to the expected Deccan direction in flow 2 (D=164.4°, I=+49.5°, α_{95}=13.5°) and flow 3 (D=169.3°, I=+52.7°, α_{95}= NA). However, flow 4 (D=126.4°, I=+44.7°, α_{95}=4.1°) and flow 5 (D=156.0°, I=+66.5°, α_{95}=8.6°) are offset 22° to the east and 19° in inclination from the Deccan mean, respectively. Literature directions for flows at Lonar and other localities in the vicinity are not statistically identical to each other or to the mean Deccan direction (grey diamonds in Fig. 5; Table 2S). Vandamme et al. (1991) argue that significant scatter between site mean directions within a single flow may be due to remaining early or late overprints (e.g., due to later reheating of the upper surfaces by succeeding flows). Only flows 4 and 5 were sampled at multiple sites separated by more than 2 km (Fig. 1); our data set is spatially and temporally too limited to average out secular variation. We conclude that the *HT* components are primary Deccan magnetization.

4.2.2. Ejecta blocks

LC_LT directions in all ejecta sites (Fig. 6a) fail the randomness test with 99% confidence (Fig. 6c) and are within 95% confidence identical

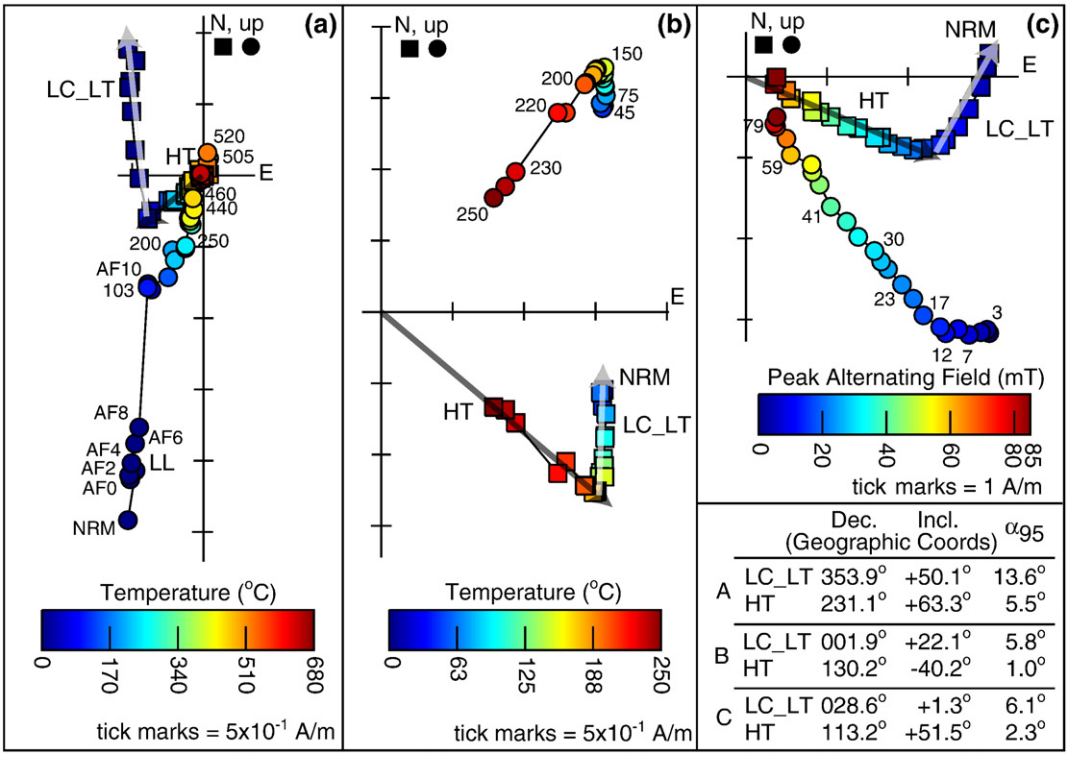

Fig. 4. Example orthogonal (Zijderveld) demagnetization plots of three specimens. Squares are 'N and E' projections, circles are 'up and E' projections. Note the differences in scales of the plots. (a) 'AF+TH' results of a background flow from Durga Devi (flow 5), (b) 'TH only' results from an ejecta block from Telcom Pit, and (c) 'Rockmag' results from a background flow at Pimplaner Dam (flow 4). See Fig. 1 and Table 1S for the geographic locations of the sites. Arrows show directional *LC-LT* and *HT* component fits: *HT* was forced through the origin. Demagnetization levels are indicated in numbers beside data points. A typical AF demagnetization sequence is: 28, 49, 72, 97, 117, 142, 171, 207, 228, 251, 276, 304, 334, 368, 405, 445, 490, 593, 652, 717, 789 and 850 mT. An example thermal demagnetization sequence is: 50, 100, 150, 200, 225, 235, 250, 275, 300, 310, 325, 340, 355, 375, 400, 420, 440, 460, 480, 505, 520, 530, 540, 560, 580, 600, 620, 630, 640, 660, and 680 °C. Color version available online.

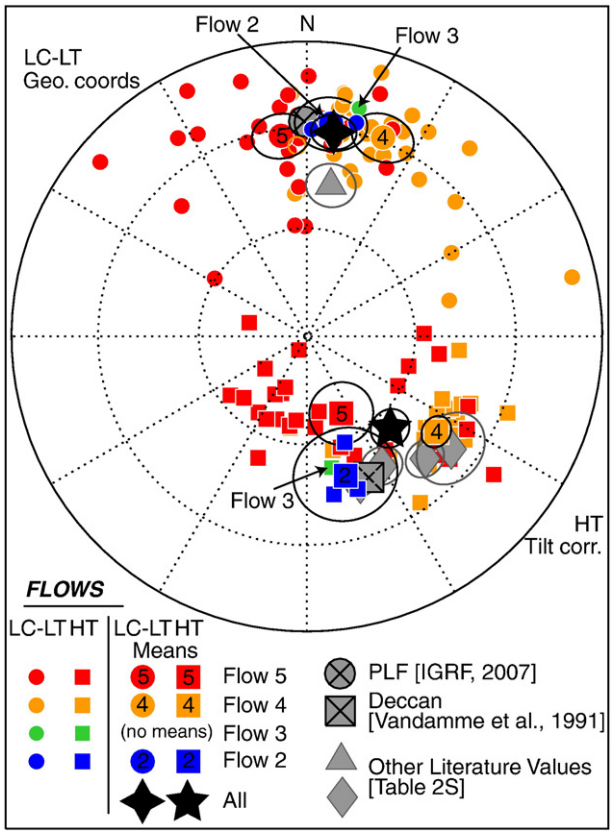

Fig. 5. Equal-area plot of magnetization fits for all flows shaded for flow number. *LC_LT* (circles) are in geographic coordinates and *HT* components (squares) are in tilt corrected coordinates. All directions are in the lower hemisphere. There is no mean or ellipse of confidence associated with flow 3 (only one sample was measured).

to the PLF. Therefore, the *LC_LT* component was acquired after ejection and deposition of the ejecta clasts. A negative result of the conglomerate test on the ejecta precludes the *LC_LT* from being an SRM (Fig. 2 and Section 2.2).

HT (Fig. 6b) passes the conglomerate test (randomness cannot be rejected) in all but one ejecta location (Fig. 6c). This result is expected if the component was acquired prior to the ejection process and randomized during deposition (Fig. 2b), and is interpreted as being primary Deccan magnetization. The *HT* component was likely not affected by SRM because its coercivity is too high (Section 5).

4.2.3. Crater rim folds

The mean *LC_LT* components (in geographic coordinates) at each of the four rim fold sites are unidirectional and identical to the PLF with 95% confidence (Figs. 6a and 3S–5S) and are also interpreted as resulting from post-impact acquisition; they fail the randomness test and the fold test, as in Fig. 2g. Pal and Ramana (1972) argued for an impact origin of Lonar based on radial dispersion of primary magnetic components in geographic coordinates in six sites along the crater rim (presumably below the hinge, from flow 4 or 5). Folding of the crater rim at Barringer (Meteor) crater, Arizona, similar in size (1.2 km diameter) and age (~50 kyr; Phillips et al., 1991) to Lonar, was observed locally along about one-third of the crater perimeter and has been likened to the peeling back of the upper layers like "the petals of a flower" (Shoemaker, 1963).

In three dimensions, the axial-surface of the fold is a flat cone with apex upward. The numerical simulation of the Lonar impact reproduces this feature well along the crater rim (Fig. 3c). However, in the numerical simulation the fold is down-warped in the lower crater walls, which is a result of crater wall slumping during modification and strongly dependent on the chosen target strength, which is variable throughout the section.

In actuality, at Lonar, initial slumping and subsequent erosion have decapitated the fold hinge along 85 to 90% of the crater rim and brecciated the hanging walls so that little intact rock is preserved in the lower half of the crater. Locally, however, the rim fold is visually and paleomagnetically preserved. One such area is the Eastern Rim site (Table 1S, Fig. 7). There, *HT* directions in geographic coordinates cluster into three groups: (1) upturned beds below the fold hinge (30–75° dip out of the crater), (2) folded beds in the fold hinge (dip>75° out of the crater), and (3) overturned rim blocks (one sample). Tilt correction of the *HT* component was performed by rotating the beds to paleohorizontal (rotation axis=bedding strike, rotation angle=bedding dip). Progressive unfolding of the *HT* component resulted in a

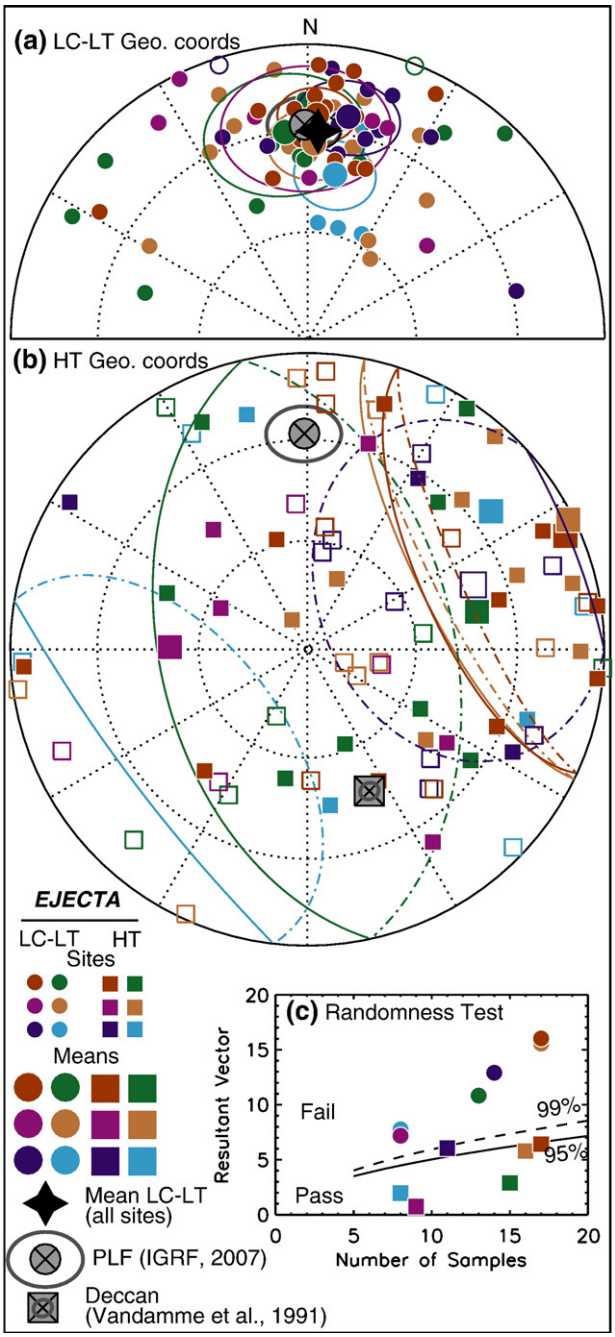

Fig. 6. Equal-area projections of (a) *LC_LT* (circles) and (b) *HT* (squares) components for all ejecta samples. Shading denotes the six ejecta sample sites. Open symbols and dash–dotted confidence ellipses denote upper hemisphere. (c) Results of a randomness test (after Watson, 1956) on the ejecta site *LC_LT* and *HT* means, solid line – 95% confidence, dashed line – 99% confidence.

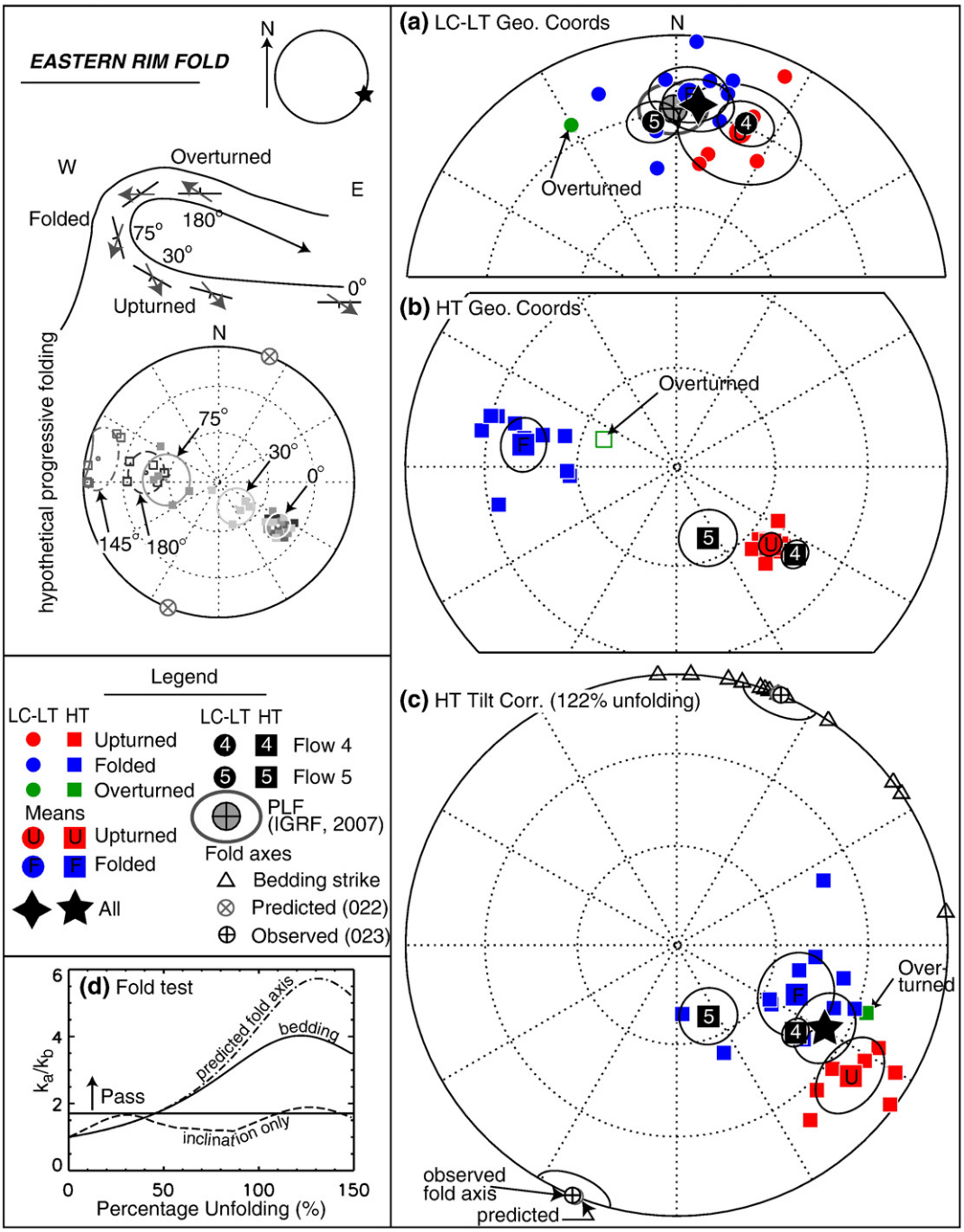

Fig. 7. Fold analysis of the Eastern Rim fold. The sampled fold consists of flow 4 (and possibly flow 5). The top left schematic indicates the location of the fold site and the hypothetical progressive change in direction of *HT* as a result of folding of flow 4 about the azimuth of the crater rim (in cross section and equal area projection). Note the switch from lower to upper hemisphere directions near 145° folding. (a) Equal-area projection of *LC_LT* (circles) in geographic coordinates, (b) equal-area projection of *HT* (squares) in geographic coordinates, and (c) equal-area projection of the *HT* components tilt corrected (squares) about the bedding strike (open triangles). Open symbols denote upper hemisphere. Specimens are subdivided into upturned, folded and overturned parts of the fold based on bedding dip (respectively 30°–75°, 75°–180°, >180°). Note that there is only one overturned specimen (open symbol in (b)) and that there is no average associated with it in (c). The mean HT components for flows 4 and 5 (Fig. 5) are shown for comparison. (d) Results of fold-test analyses (precision parameter k_a relative to the initial k_b): solid line = unfolding about the individual sample bedding by the dip; dash-dot line = folding about the predicted fold axis (crater rim azimuth) by the dip; dashed line = inclination only results of folding about the bedding by the dip.

continuous increase of the precision parameter (k, a measure of the clustering of the magnetic vectors; Fisher, 1953) by a factor of 3.7 upon 100% unfolding and a maximum of 4.0 at 122% unfolding (Fig. 7c and d; after McElhinny, 1964). The fold test results after 100% and 122% are statistically identical to each other with 95% confidence and a minimum of 45% unfolding is required to pass the fold test. The site mean *HT* after 122% tilt correction (D = 112.5°, I = +50. 8°, α_{95} = 11.9°) is statistically identical to the local mean of flow 4, although the cluster groups (1–3) remained statistically distinct from each other. The sampled fold consists of flows 4 and 5, which are statistically different from each other (Fig. 7 and Table 2S). If the original magnetic directions were all the same, then we would expect the maximum increase in k to occur at 100% unfolding; the combined precision parameter is only an approximate indicator of commonality.

Along the Southern Rim (Fig. S3), the *HT* component also passes the fold test upon 83% tilt correction. Locally we can approximate the crater rim fold as a cylindrical, horizontal fold with a predicted fold axis parallel to the rim. On the eastern rim the average measured

bedding strike (observed fold axis) is 025° and the azimuth of the crater rim (predicted fold axis) is 022°; on the southern rim they are 077° and 075° respectively.

Elsewhere, the simple cylindrical fold approximation cannot be made. On the Northwestern Rim (Fig. 4S) after tilt correction *HT* vectors do not pass the fold test. If we ignore the horizontal components of the magnetic directions, and only consider the improvement in clustering of the inclinations (vertical components), then the site does pass an 'inclination only' fold test with 99% confidence. A minimum of 30° of additional clockwise rotation of three samples on the rim is sufficient for the region to pass a proper fold test. At Barringer crater, a small number of nearly vertical tear faults with scissors-type displacement, disrupt the crater rim fold (Shoemaker, 1963). Although no tear faults were identified at Lonar crater (Maloof et al., in press), tearing in the overturned rim flap is inferred from paleomagnetic observations of the rim blocks. At the Western Rim site (Fig. 5S) the blocks have become too jumbled during rollover for conventional fold tests to describe their behavior. In fact, the rotated rim block samples are statistically random, indicating a conglomerate test may be more appropriate in chaotic regions of the fold.

5. Discussion

5.1. The nature of the LC_LT component

Our paleomagnetic results show that the primary magnetization is preserved in the *HT* component in all the groups and that it is similar to the local Deccan flow direction, but not identical to the paleo-Deccan direction from the literature (Table 2S). *LC_LT* directions were found to be statistically identical to the PLF in all groups. Since SRM would result in randomization of the *LC_LT* in the ejecta blocks (Figs. 2 and 6), as well as in the folded rim rocks (Figs. 2 and 7), we interpret the *LC_LT* in all groups as a post-impact viscous remanent magnetization (VRM) and/or chemical remanent magnetization (CRM). An 'intermediate' magnetic component (between *LC_LT* and *HT*) was not identified in this data set. Below, we investigate whether a post-impact magnetization may have (completely) replaced any original SRM, based on magnetic intensity, unblocking temperature and coercivity considerations.

We define the relative intensity of *LC_LT* as the moment fraction it occupies in the entire NRM demagnetization path, or $|LC\_LT|/(|LC\_LT| + |HT|)$, where $|\ |$ denotes the vector length of the demagnetization path. Histograms of this parameter are shown, per site group, in Fig. 8.

LC_LT fractions are generally below 0.4 in all the groups, although often higher, and occasionally as high as 0.85. A compilation of published example Zijderveld plots of Deccan lavas from sites not associated with an impact crater (Vandamme et al., 1991; Vandamme and Courtillot, 1992; Courtillot et al., 2000) indicate similar means and ranges, and are occasionally greater than 0.95 (Vandamme and Courtillot, 1992) as well.

The unblocking temperatures of the secondary component (Fig. 9a), identified by an inflection in the orthogonal projections in results from 'TH only' experiments (Fig. 4b), are in all groups within 1σ of the mean of the unshocked background flows (187 ± 15 °C). Since shock heating is not expected to be more than a few tens of degrees in all but a few of the ejecta blocks (see Section 2.3), the unblocking temperature cannot be attributed to shock heating. The unblocking temperature agrees well with secondary components in studies of other Deccan lavas (on average 200 °C; Vandamme et al., 1991; Courtillot et al., 2000). Blocking diagram calculations for single-domain magnetite (Pullaiah et al., 1975) suggest that magnetic fractions which are unblocked at 187 °C by heating for 30 min in the laboratory have relaxation (~ viscous acquisition) timescales of 4 years at 100 °C and are on the order of the age of the crater at temperatures slightly above surface temperature (50 kyr at 50 °C, see Fig. 1a in Pullaiah et al., 1975). The inferred timescales are upper estimates as the Lonar basalts are not purely single-domain.

Alternating field demagnetization of NRM experiments ('AF+RM' experiments, Fig. 4c) resulted in coercivities of the *LC_LT* between 5 and 23 mT (Fig. 9b). *LC_LT* in the background flows is relatively weak (around 12 mT) compared to the other groups. However, it should be noted that these specimens were collected from fresh quarries only and are likely less weathered than rocks collected at the surface in the other groups. Other studies of basalts at Lonar indicate *LC_LT* unblocking ranges of 10 to 20 mT (Nishioka et al., 2007). The secondary component in Deccan basalts from other locations was generally erased between 5 and 7.5 mT, but occasionally required fields between 10 and 20 mT as well (Athavale and Anjaneyulu, 1972; Vandamme et al., 1991; Courtillot et al., 2000).

Our VRM acquisition experiments for Lonar basalts ('VRMacq' experiments, Fig. 6S), when extrapolated to the age of the crater, predict natural VRM intensities (Table 3S), spanning the range of *LC_LT* observed in Fig. 8. Although the estimated VRM fractions are generally below 0.16, one ejecta block sample did reach 0.89. The relative intensity (as well as direction), coercivity, and blocking temperature of *LC_LT* compared to

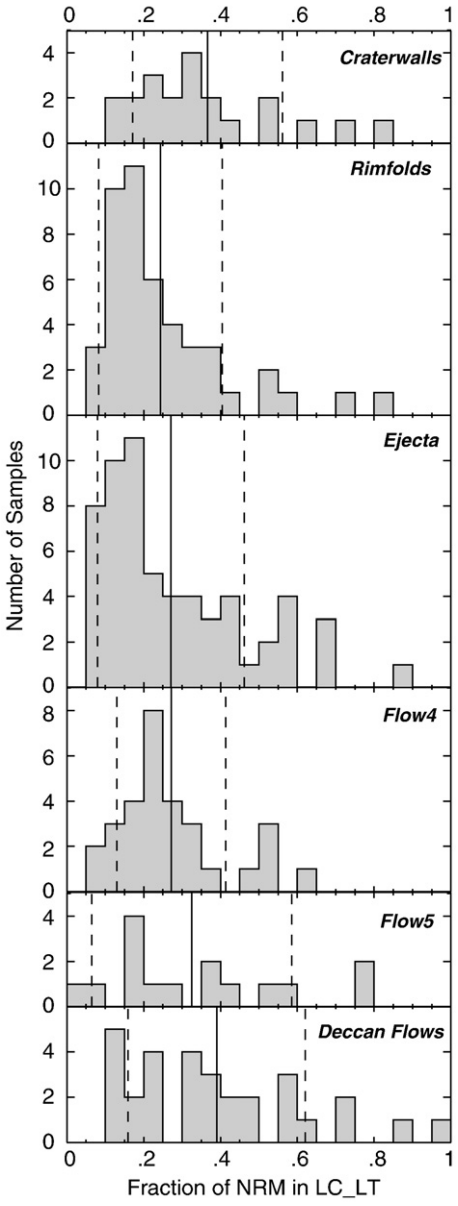

Fig. 8. Histograms showing the fraction of NRM contained by the *LC_LT* component, $|LC\_LT|/(|LC\_LT| + |HT|)$, in the crater walls, rim folds, ejecta, background flows 4 and 5 at Lonar crater, and other Deccan flows from the literature (Vandamme et al., 1991; Vandamme and Courtillot, 1992; Courtillot et al., 2000). Vertical solid lines = mean, dashed lines = mean +/− 1σ. The histograms combine results from 'AF+TH', 'TH only' and 'Rockmag' experiments.

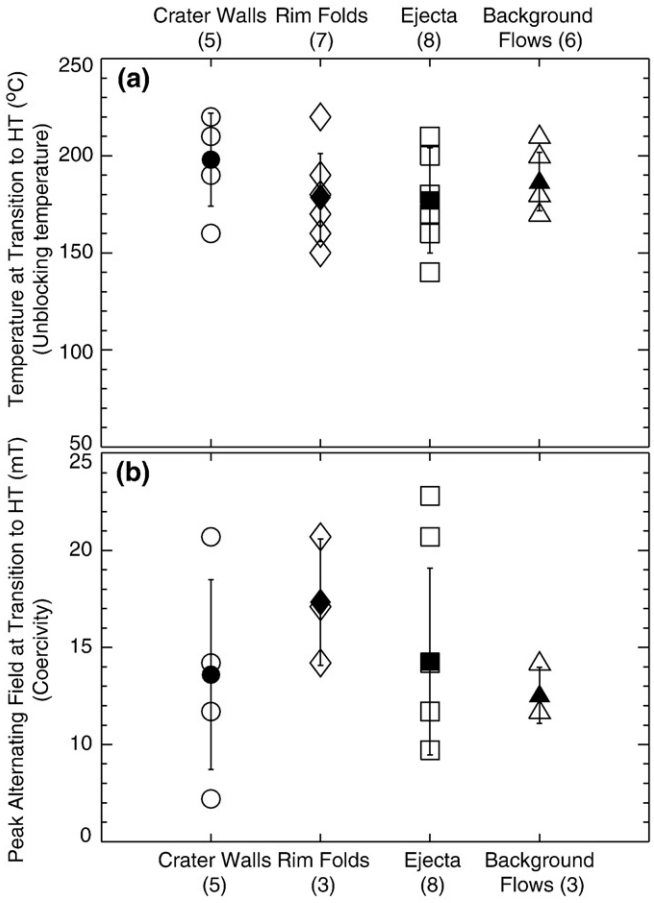

Fig. 9. (a) Unblocking temperatures in degrees Celsius ('TH only') and (b) peak alternating fields in mT ('AF+RM') at the transition to the *HT* components. The errors are on the order of the step size (10 °C and 2–3 mT). Open symbols indicate individual measurements; solid symbols indicate site type means ± 1σ. The number of samples in each group is indicated in parentheses.

those of other Deccan basalts, lead us to conclude that the acquisition mechanism (VRM (Courtillot et al., 2000) and/or CRM) is the same for all. Impact-related hydrothermal alteration at Lonar was generally greatest below the crater floor and likely did not exceed 200 °C (Hagerty and Newsom, 2003; Newsom et al., 2007). However, low temperature alteration of Deccan basalts is common (e.g. Schaal, 1976; Gwalani, 1981). At Lonar, basalt flows are often separated by paleosols and/or deeply altered, feruginized flow top autobreccia ("red boles", Kieffer et al., 1976; Murali et al., 1987) indicating that extensive contemporaneous and post-impact weathering would have contributed to alteration of the rocks. Of the alteration minerals that comprise less than 10% of the massive interiors of flows, hematite is the dominant magnetic phase (Kieffer et al., 1976; Schaal, 1976; Vandamme and Courtillot, 1992). The lack of significant NRM blocked above 580 °C, and the little change in magnetization after cycling through the transition at −15 °C (Morin, 1950) in a magnetically shielded space (compare the dark and light grey symbols in Fig. 2S), indicate that the *LC_LT* component is not controlled by hematite. VRM acquisition is likely the dominant mechanism of secondary magnetic overprint at Lonar.

5.2. Magnetic shock indicators

Even though the unblocking temperature of the *LC_LT* component cannot be attributed to shock, it does provide an upper limit on the amount of shock heating. Petrographic indicators of shock in the paleomagnetically studied rocks from Lonar are sparse. Only plagioclase and (occasionally olivine) form euhedral phenocrysts that are sufficiently large for petrographic study. Postdepositional alteration to clays renders olivine birefringence nearly useless at Lonar. Fortuitously, two ejecta block thin sections from the Telcom Pit site showed signs of stress in the form of undulose extinction in plagioclase and irregular cracks in olivine phenocrysts (Fig. 7S). Comparisons with shock experiments on feldspars (Gibbons and Ahrens, 1977) and shocked chondrites (Stöffler et al., 1991, Schmitt and Stöffler, 1995) suggest a shock pressure between 5 and 30 GPa. New, in situ, post-shock temperature measurements on Columbia River basalts range between 184 and 472 °C for shocks between 5 and 25 GPa (Stewart et al., 2007).

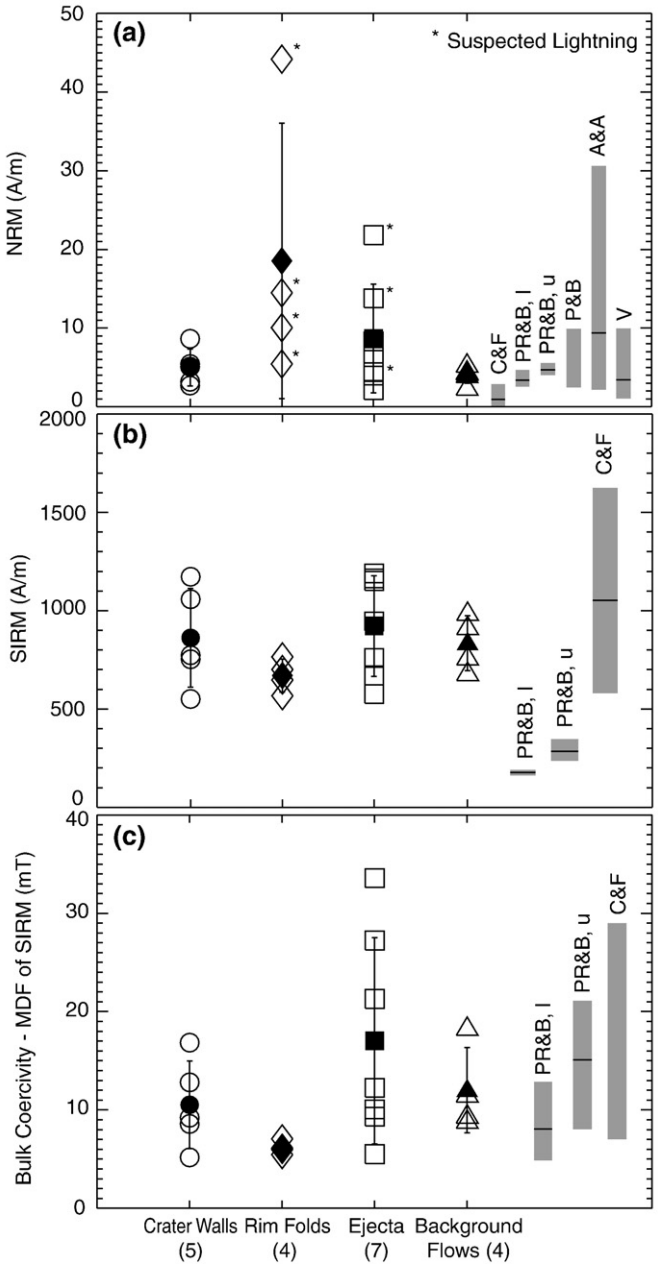

Fig. 10. (a) Natural remanent magnetization (NRM) defined as the total length of the demagnetization path (|*LC_LT*|+|*HT*|), (b) saturation isothermal remanent magnetization (SIRM) acquired in a 1 T field, and (c) median destructive field (MDF) of SIRM (the field required to reduce the SIRM by 50%) of the Lonar basalts. An average basalt density of 2.9 g/cm^3 (Fudali et al., 1980) was assumed. Open symbols denote individual samples; filled symbols denote the site type mean ± 1σ with the number of samples indicated in parentheses. Symbols with an asterisk in (a) denote specimens where lightning may have affected the magnetic intensities. Shaded regions indicate literature value ranges (with means): C&F = Lonar crater (Cisowski and Fuller, 1978); PR&B u = upper and l = lower flows in Lonar crater (Poornachandra Rao and Bhalla, 1984); V = Nagpur-Bombay (Vandamme et al., 1991); A&A = Aurangabad (Athavale and Anjaneyulu, 1972); and P&B = Jalna (Pal and Bhimasankaram, 1971).

Unblocking temperatures of approximately 200 °C therefore limit shock pressures in these specimens to the lower end of the shock pressure range indicated by the petrographic observations. Paleomagnetism is a potentially useful indicator of shock intensity, in particular an upper limit on heating, but also pressure, when petrographic observations are sparse or compromised because of alteration.

Magnetic rocks and minerals can undergo the following rock-magnetic changes as a result of shock: (1) demagnetization resulting in a reduction of NRM, (2) increasing saturation isothermal remanence (SIRM), and (3) increasing coercivity (e.g., Cisowski and Fuller, 1978; Pesonen et al., 1997; Gattacceca et al., 2007b; Louzada et al., 2007). Mean NRM intensities (here presented as the total length of the demagnetization path, $|LC\_LT| + |HT|$, Fig. 10a) of the crater wall and ejecta blocks are within error of those of the background flows from this and other studies and nearby Deccan basalts (Table 4S) arguing against significant shock demagnetization. Note that care should be taken when interpreting NRM, which is a result of more than one magnetic component. An altitudinal dependence on shock demagnetization in the crater walls (Poornachandra Rao and Bhalla, 1984; Nishioka et al., 2006) is not expected from the model results in Section 2.3, and could be explained by differing mineralogical content and extent of weathering between the lower and upper flows. We interpret the relatively high mean NRM of the crater rim folds as being largely due to two samples with anomalous magnetic declinations as a result of lightning strikes. We find no evidence of intense impact-generated or amplified magnetic fields. Impact glasses and spherules are also inefficiently magnetized (Weiss et al., 2007), possibly either because they cooled after the field has decayed away or randomization of the magnetic vector resulting from translation and rotation during flight.

There are no striking differences in SIRM between the different groups (Fig. 10b), but there are in the median destructive field of SIRM (MDF of SIRM, Fig. 10c). MDF is the peak alternating field required to demagnetize a sample by 50%, a measure of the bulk coercivity, and has been shown to increase in magnetite in both static (up to 6 GPa; Gilder et al., 2004; Gilder and Le Goff, 2008) and shock experiments (up to 35 GPa; Pesonen et al., 1997). MDF of SIRM is generally below 20 mT in all groups, but not in some of the ejecta clasts (Fig. 8Sa). The ejecta have both the largest range and highest average value of MDF of SIRM. Since, the ejecta are a collection of unshocked and shocked clasts, the large range of coercivities is possibly indicating the effects of shock.

The rock-magnetic evidence for shock at Lonar remains subtle. This result is likely because the shock pressures were low and the primary magnetization is confined to thermoremanent magnetization in high coercivity fractions (note the high MDF of NRM in Fig. 8Sb and Table 4S) where low pressure shock modification is inefficient (e.g. Gattacceca et al., 2007a). The best candidate samples for recording shock effects on magnetization are the highest shocked ejecta.

Since shocked rocks constitute only a small percentage of rocks in the ejecta blanket, the effects of shock are diluted when the blanket is studied as a whole.

6. Implications

Cisowski and Fuller (1978) concluded that the variability of remanence in the Deccan basalts from Lonar can be explained in terms of their differing response to shock as a function of coercivity. Due to the lack of oriented samples, they could not determine whether or not the secondary component was shock-induced. Here, we have shown that the mean *LC_LT* is statistically identical to the present-day local field and that most (or all) of any primary SRM has been obscured by VRM (and CRM) in the time elapsed since the impact event. Given that Lonar is one of the youngest and best preserved craters on Earth, we suggest that SRM may not be preserved in small terrestrial craters. Hargraves and Perkins (1969), but not Cisowski and Fuller (1978), concluded similarly at Barringer crater. At larger craters, such as Bosumtwi, Ghana (~10.5 km diameter, Elbra et al., 2007), Ries, Germany (22–23 km diameter, Pohl and Angenheister, 1969), Rochechouart, France (23 km diameter, Carporzen and Gilder, 2006), and Slate Islands, Canada (~30 km diameter, Halls, 1975; Halls, 1979), shock remanent magnetization has been inferred in more intensely shocked rocks, such as frictionally heated breccia.

Unless SRM is acquired as TRM in melt rocks and sheets, or in shock-produced grains in the presence of impact-generated fields, it will not be preserved. It was a lack of oriented ejecta blocks that led Poornachandra Rao et al. (1984) to argue for SRM at Lonar, and that the *LC_LT* component could be used to constrain the age of the impact event. The susceptibility of SRM to post-impact remagnetization and its inherent predicted spatial and directional complexity indicate that SRM is generally not a suitable crater-age dating tool; unless it was acquired as a TRM during cooling of melt rocks after an impact-generated field has decayed.

Aerial magnetic surveys of terrestrial impact craters with diameters smaller than 10 km often have magnetic low anomalies (Pilkington and Grieve, 1992). In uneroded structures, these magnetic lows may be due to the reduction of magnetization (remanent and/or induced) intensity and/or randomization of magnetic moments (e.g. the randomization of the primary components in the ejecta). Intense magnetization and randomization at Vredefort has been attributed to TRM acquired in impact-amplified or impact-generated fields in magnetite confined to planar deformation features in shocked quartz grains (Cloete et al., 1999; Carporzen et al., 2005). The lack of evidence of impact-generated fields at Lonar suggests that fields much greater than Earth strength are difficult to generate from Lonar-sized impact events, or that the impact-generated fields are too short-lived or spatially confined to be recorded. A numerical estimate of impact-field intensities based on laboratory studies for the Lonar impact scenario (Section 2.3) is ~7 μT (Eq. (8); Crawford and Schultz, 1999).

Inside the Martian impact basins Hellas (~1400 diameter) and Argyre (~1100 km diameter), where shock pressures and temperatures were great enough to induce complete melting, the absence of crustal magnetic anomalies argues for the absence of a global magnetic field and the rapid and early shutdown of the Martian core dynamo (Acuña et al., 1999; Lillis et al., 2008). Partial demagnetization of the Martian crust up to ~1.4 basin radii (Hood et al., 2003; Mohit and Arkani-Hamed, 2004) has been attributed to the low pressure (a few GPa) demagnetization of the crust, in the absence of an ambient field. The results from Lonar suggest that in the presence of a weak field like that of the Earth, SRM and shock demagnetization are obscured by post-impact magnetic acquisition.

7. Conclusions

We have conducted paleomagnetic and rock-magnetic studies of oriented basalts from a terrestrial analogue of craters on other terrestrial planets and the Moon, in order to test for changes in magnetic remanence and properties as a result of shock. The basalts at Lonar crater contain two stable magnetic components: a low coercivity/low temperature (*LC_LT*) component and a high temperature (*HT*) component. The *HT* component is similar to the mean Deccan direction, though slightly offset (0 to 21°) due to limited sampling of secular variation, and is interpreted as a primary magnetization acquired during cooling of the lavas approximately 65 Ma. The *LC_LT* component is a post-impact magnetic overprint acquired since the formation of the crater and is statistically identical to the present-day local magnetic field. In this study, we suggest that negative conglomerate test results on the secondary component in ejecta blocks and folded rim blocks rule out the presence of shock remanent magnetization. We conclude that any shock remanent magnetization acquired during the impact was replaced by post-impact viscous and/or chemical remanent magnetization. Impact-generated and impact-amplified fields are probably only preserved in much larger craters, where they could be recorded either in shock-

produced grains or as a thermoremanent magnetization in extensive melt sheets.

Paleomagnetism is a useful tool for studying impact tectonics and shock intensity. Paleomagnetic fold tests indicate that locally the crater rim fold can be approximated by a horizontal cylindrical fold parallel to the crater rim (in the eastern and southern rim). In other places the fold is disrupted due to tearing, indicating additional vertical axis rotation (~30°) has occurred, as would be expected in a radial fold. Paleomagnetism also provides an upper limit on shock heating, and indirectly shock pressure, when petrographic indicators are sparse or compromised because of alteration. For Lonar crater, we find that shock heating did not exceed ~200 °C in the crater wall and ejecta blocks.

Rock-magnetic effects of shock are subtle at Lonar. However, greater bulk coercivity in some ejecta blocks relative to the unshocked background basalts is a potential shock indicator that warrants further development.

Acknowledgements

Thank you to H. Newsom, S. Wright, J. Kirschvink, R. Kopp, I. Hilburn, L. Carporzen, I. Garrick-Bethell, L. Senft, J. Gattacceca, T. Kohout, E. Mervine, A. Misra, M. Funaki, and F. Hörz for helpful discussions, sample collection, laboratory training and support, and D. Dunlop and G. Osinksi for constructive reviews. This work was generously supported by the Harvard University Department of Earth and Planetary Sciences, NASA MFRP Grants #NNG06GH34G (S.T.S.) and #NNX06AD14G (B.P.W.), and the Zonta International Amelia Earhart Fellowship (K.L.L.).

Appendix A. Supplementary data

Supplementary data associated with this article can be found, in the online version, at doi:10.1016/j.epsl.2008.08.025.

References

Acuña, M.H., Connerney, J.E.P., Ness, N.F., Lin, R.P., Mitchell, D., Carlson, C.W., McFadden, J., Anderson, K.A., Rème, H., Mazelle, C., Vignes, D., Wasilewski, P., Cloutier, P., 1999. Global distribution of crustal magnetization discovered by the Mars Global Surveyor MAG/ER experiment. Science 284, 790–793.

Athavale, R.N., Anjaneyulu, G.R., 1972. Palaeomagnetic results on Deccan Trap lavas of the Aurangabad region and their tectonic significance. Tectonophysics 14, 87–103.

Bezaeva, N.S., Rochette, P., Gattacceca, J., Sadykov, R.A., Trukhin, V.I., 2007. Pressure demagnetization of the Martian crust: ground truth from SNC meteorites. GRL 34. doi:10.1029/2007GL031501.

Carporzen, L., Gilder, S.A., Hart, R.J., 2005. Palaeomagnetism of the Vredefort meteorite crater and implications for craters on Mars. Nature 435, 198–201.

Carporzen, L., Gilder, S.A., 2006. Evidence for coeval Late Triassic terrestrial impacts from Rochechouart (France) meteorite crater. GRL 33. doi:10.1029/2206GL027356.

Cisowski, S.M., Fuller, M., 1978. The effect of shock on the magnetism of terrestrial rocks. JGR 83, 3441–3458.

Cloete, M., Hart, R.J., Schmid, H.K., Drury, M., Demanet, C.M., Sankar, K.V., 1999. Characterization of magnetite particles in shocked quartz by means of electron- and magnetic force microscopy: Vredefort, South Africa. Contrib. Mineral. Petrol. 137, 232–245.

Courtillot, V., Gallet, Y., Rocchia, R., Féraud, G., Robin, E., Hofmann, C., Bhandari, N., Ghevariya, Z.G., 2000. Cosmic markers, $^{40}Ar/^{39}Ar$ dating and paleomagnetism of the KT sections in the Anjar Area of the Deccan large igneous province. EPSL 182, 137–156.

Crawford, A.R., 1983. Mantle convection pattern under India: relevance to Lonar crater, Girnar node and peri-Indian volcanism. J. Geol. Soc. India 24, 97–100.

Crawford, D.A., Shultz, P.H., 1988. Laboratory investigations of impact-generated magnetic-fields. Nature 3, 50–52.

Crawford, D.A., Schultz, P.H., 1991. Laboratory investigations of impact-generated plasma. JGR 96, 18,807–818,817.

Crawford, D.A., Schultz, P.H., 1993. The production and evolution of impact-generated magnetic fields. Int. J. Impact Eng. 14, 205–216.

Crawford, D.A., Schultz, P.H., 1999. Electromagnetic properties of impact-generated plasma, vapor and debris. Int. J. Impact Eng. 23, 169–180.

Elbra, T., Kontny, A., Pesonen, L.J., Schleifer, N., Schell, C., 2007. Petrophysical and paleomagnetic data of drill cores from the Bosumtwi impact structure, Ghana. MAPS 42, 829–838.

Elmaleh, A., Valet, J.-P., Quidelleur, X., Solihin, A., Bouquerel, H., Tesson, T., Mulyadi, E., Khokhlov, A., Wirakusumah, A.D., 2004. Palaeosecular variation in Java and Bawean Islands (Indonesia) during the Bruhnes chron. GJI 157, 441–454.

Evans, M.E., Wayman, M.L., 1974. An investigation of the role of ultrafine titanomagnetite intergrowths in paleomagnetism. Geophys. J. R. Astron. Soc. 36, 1–10.

Fisher, R., 1953. Dispersion on a sphere. Proc. R. Soc. Lond., A Math. Phys. Sci. 217, 295–305.

Fredriksson, K., Dube, A., Milton, D.J., Balasundaram, M.S., 1973a. Lonar Lake, India: an impact crater in basalt. Science 180, 862–864.

Fredriksson, K., Noonan, A., Nelen, J., 1973b. Meteoritic, lunar and Lonar impact chondrules. Moon 7, 475–482.

Fudali, R.F., Milton, D.J., Fredriksson, K., Dube, A., 1980. Morphology of Lonar crater, India: comparisons and implications. Moon Planets 23, 493–515.

Gattacceca, J., Berthe, L., Boustie, M., Vadeboin, F., Rochette, P., De Resseguier, T., 2007a. On the efficiency of shock remanent processes. PEPI. doi:10.1016/j.pepi.2007.1009.1005.

Gattacceca, J., Lamali, A., Rochette, P., Boustie, M., Berthe, L., 2007b. The effects of explosive-driven shocks on the natural remanent magnetization and the magnetic properties of rocks. PEPI. doi:10.1016/j.pepi.2007.1003.1006.

Gibbons, R.V., Ahrens, T.J., 1977. Effects of shock pressures on calcic plagioclase. Phys. Chem. Miner. 1, 95–107.

Gilbert, G.K., 1896. The origin of hypotheses, illustrated by the discussion of a topographic problem. Science 3, 1–13.

Gilder, S.A., LeGoff, M., Chervin, J.-C., Peyronneau, J., 2004. Magnetic properties of single and multi-domain magnetite under pressures from 0 to 6 GPa. GRL 31. doi:10.1029/2004GL019844.

Gilder, S.A., Le Goff, M., 2008. Systematic pressure enhancement of titanomagnetite magnetization. GRL 35. doi:10.1029/2008GL033325.

Grieve, R.A.F., Garvin, J.B., Coderre, J.M., Rupert, J., 1989. Test of a geometric model for the modification stage of simple impact crater development. Meteoritics 24, 83–88.

Gwalani, L.G., 1981. Petrology of Deccan Traps and Bagh Beds of Dugdha-Naswadi, Gujarat. Somaiya Publications Pvt. Ltd., Bombay.

Hagerty, J.J., Newsom, H.E., 2003. Hydrothermal alteration at the Lonar Lake impact structure, India: implications for impact cratering on Mars. MAPS 38, 365.

Halls, H.C., 1975. Shock-induced remanent magnetisation in late Precambrian rocks from Lake Superior. Nature 255, 692–695.

Halls, H.C., 1979. The Slate Islands meteorite impact site: a study of Shock Remanent Magnetization. Geophys. J. R. Astron. Soc. 59, 553–591.

Hargraves, R.B., Perkins, W.E., 1969. Investigations of the effect of shock on natural remanent magnetization. JGR 74, 2576–2589.

Hart, R.J., Hargraves, R.B., Andreoli, M.A.G., Tredoux, M., Doucouré, C.M., 1995. Magnetic anomaly near the center of the Vredefort structure: Implications for impact-related magnetic signatures. Geology 23, 277–280.

Hood, L.L., Richmond, N.C., Pierazza, E., Rochette, P., 2003. Distribution of crustal magnetic fields on Mars: Shock effects of basin-forming impacts. GRL 30, 1281–1284.

IGRF, International Geomagnetic Reference Field, 2007.

Kieffer, S.W., Schaal, R.B., Gibbons, R., Horz, F., Milton, D.J., Dube, A., 1976. Shocked basalt from Lonar Impact Crater, India, and experimental analogues. LPSC 7th, 1391–1412.

Kirschvink, J.L., 1980. The least-squares line and plane and the analysis of palaeomagnetic data. Geophys. J. R. Astron. Soc. 62, 699–718.

Kletetschka, G., Connerney, J.E.P., Ness, N.F., Acuña, M.H., 2004. Pressure effects on Martian crustal magnetization near large impact basins. MAPS 39, 1839–1848.

Kumar, P.S., 2005. Structural effects of meteorite impact on basalt: evidence from Lonar Crater, India. JGR 110. doi:10.1029/2005JB003662.

La Touche, T.H.D., Christie, W.A.K., 1912. The geology of Lonar Lake — with a note on the Lonar soda deposit. Rec. Geol. Surv. India 41, 266–285.

Lafond, E.C., Dietz, R.S., 1964. Lonar Crater, India, a meteorite crater? Meteoritics 2, 111–116.

Lillis, R.J., Frey, H.V., Manga, M., 2008. Rapid decrease in Martian crustal magnetization in the Noachian era: implications for the dynamo and climate of early Mars. GRL 35. doi:10.1029/2008GL034338.

Lin, R.P., Mitchell, D.L., Curtis, D.W., Anderson, K.A., Carlson, C.W., McFadden, J., Acuña, M.H., Hood, L.L., Binder, A., 1998. Lunar surface magnetic fields and their interaction with the solar wind: results from lunar prospector. Science 281, 1480–1484.

Louzada, K.L., Stewart, S.T., Weiss, B.P., 2007. Effect of shock on the magnetic properties of pyrrhotite, the Martian crust, and meteorites. GRL 34. doi:10.1029/2006GL027685.

Maloof, A.C., Stewart, S.T., Weiss, B.P., Soule, S.A., Swanson-Hysell, N., Louzada, K.L., Poussart, P.M., Garrick-Bethell, I., in press. Geology of Lonar Crater, India. GSA Bulletin

McElhinny, M.W., 1964. Statistical significance of the fold-test in paleomagnetism. Geophys. J. R. Astron. Soc. 8, 338–340.

McGlaun, J.M., Thompson, S.L., Elrick, M.G., 1990. CTH: a 3-dimensional shock-wave physics code. Int. J. Impact Eng. 10, 351–360.

Melosh, H.J., 1989. Impact Cratering: A Geologic Process. Oxford University Press, New York.

Melosh, H.J., Beyer, R.A., 1998. Crater Program. http://www.lpl.arizona.edu/tekton/crater.html.

Mohit, P.S., Arkani-Hamed, J., 2004. Impact demagnetization of the Martian crust. Icarus 168, 305–317.

Morin, F.J., 1950. Magnetic susceptibility of αFe_2O_3 and αFe_2O_3 with added titanium. Phys. Rev. 78, 819–820.

Murali, A.V., Zolensky, M.E., Blanchard, D.P., 1987. Tektite-like bodies at Lonar crater, India: implications for the origin of tektites. JGR 92, E729–E735.

Nagata, T., 1971. Introductory notes on shock remanent magnetization and shock demagnetization of igneous rocks. Pure Appl. Geophys. 89, 159–177.

Nakazawa, S., Watanabe, S., Kato, M., Iijima, Y., Kobayashi, T., Sekine, T., 1997. Hugioniot equation of state of basalt. Planet. Space Sci. 45, 1489–1492.

Nayak, V.K., 1972. Glassy objects (impact glasses?) a possible new evidence for meteoritic origin of the Lonar crater, Maharashtra State, India. EPSL 14, 1–6.

Nayak, V.K., 1993. Maskelynite from the Indian impact crater at Lonar. J. Geol. Soc. India 41, 307–312.

Newsom, H.E., Misra, S., Nelson, M.J., 2007. Aqueous Alteration of the Proximal and Distal Ejecta Blanket at Lonar Crater, India, Lunar and Planetary Science Conference XXXVIII, Houston, TX. 2056.

Nishioka, I., Funaki, M., Rao, V., 2006. Shock demagnetization of basalt from Lonar impact crater in India. AGU 2006 Fall Meeting, AGU, San Francisco, p. GP11B-0081.
Nishioka, I., Funaki, M., Venkata Rao, K., 2007. Paleomagnetism of Basalts from Lonar impact crater. 70th Annual Meteoritical Society Meeting, Tuscon, Arizona. 5179.
Pal, P.C., Bhimasankaram, V.L.S., 1971. Palaeomagnetism of the Deccan Trap flows of Jalna, India. EPSL 11, 109–112.
Pal, P.C., Ramana, C.V., 1972. Lonar lake — volcanic crater or astrobleme. C.E.G. Bulletin 114–121.
Pesonen, L.J., Deutsch, A., Hornemann, U., Langenhorst, F., 1997. Magnetic properties of diabase samples shocked experimentally in the 4.5 to 35 GPa range. LPSC XXVIII, 1087–1088.
Phillips, F.M., Zreda, M.G., Smith, S.S., Elmore, D., Kubik, P.W., Dorn, R.I., Roddy, D.J., 1991. Age and geomorphic history of Meteor Crater, Arizona, from cosmogenic ^{36}Cl and ^{14}C in rock varnish. Geochim. Cosmochim. Acta 55, 2695–2698.
Pierazzo, E., Vickery, A.M., Melosh, H.J., 1997. A reevaluation of impact melt production. Icarus 127, 408–423.
Pilkington, M., Grieve, R.A.F., 1992. The geophysical signature of terrestrial impact craters. Rev. Geophys. 30, 161–181.
Pohl, J., Angenheister, G., 1969. Anomalien des Erdmagnetfeldes und Magnetisierung der Gesteine im Nördlinger Ries. Geol. Bavarica 61, 327–336.
Poornachandra Rao, G.V.S., Bhalla, M.S., 1984. Lonar lake: palaeomagnetic evidence of shock origin. Geophys. J. R. Astron. Soc. 77, 847–862.
Pullaiah, G., Irving, E., Buchan, K.L., Dunlop, D.J., 1975. Magnetization changes caused by burial and uplift. EPSL 28, 133–143.
Schaal, R.B., 1976. Shock Metamorphism in Basalt from Lonar Crater, India, and in Six Lunar Microcraters. University of California, Los Angeles.
Senft, L.E., Stewart, S.T., 2007. Modeling impact cratering in layered surfaces. JGR 112. doi:10.1029/2007JE002894.
Sengupta, D., Bhandari, N., Watanabe, S., 1997. Formation age of Lonar meteor crater, India. Rev. Fís. Apl. Instrum. 12, 1–7.
Shoemaker, E.M., 1963. Impact mechanics at Meteor crater, Arizona. In: Middlehurst, B.M., Kuiper, G.P. (Eds.), The Moon, Meteorites and Comets. University of Chicago Press, Chicago, pp. 301–336.
Schmitt, R.T., Stöffler, D., 1995. Classification of Chondrites. Meteoritics 30, 574–575.
Son, T.H., Koeberl, C., 2007. Chemical variation in Lonar impact glasses and impactites. GFF 129, 161–176.
Srnka, L.J., Martelli, G., Newton, G., Cisowski, S.M., Fuller, M.D., Schaal, R.B., 1979. Magnetic field and shock effects and remanent magnetization in a hypervelocity experiment. EPSL 42, 127–137.
Stewart, S.T., Seifter, A., Kennedy, G.B., Furlanetto, M.R., Obst, A.W., 2007. Measurements of emission temperatures from shocked basalt: hot spots in meteorites. Lunar Planet. Sci. XXXVIII, 2413.
Stöffler, D., Keil, K., Scott, E.R.D., 1991. Shock metamorphism of ordinary chondrites. Geochimica et Cosmochimica Acta 55, 3845–3867.
Stroube Jr., W.B., Garg, A.N., Ali, M.Z., Ehmann, W.D., 1978. A chemical study of the impact glasses and basalts from Lonar crater, India. Meteoritics 13, 201–208.
Subrahmanyam, B., 1985. Lonar crater, India: a crypto-volcanic origin. J. Geol. Soc. India 26, 326–335.
Szabó, E., Halls, H.C., 2006. Deformation of the Sudbury structure: paleomagnetic evidence from the Sudbury breccia. Precambrian Res. 150, 27–48.
Urrutia-Fucugauchi, J., Soler-Arechalde, A.M., Rebolledo-Vieyra, M., Vera-Sanchez, P., 2004. Paleomagnetic and rock magnetic study of the Yaxcopoil-1 impact breccia sequence, Chicxulub impact crater (Mexico). MAPS 39, 843–856.
Vandamme, D., Courtillot, V., 1992. Paleomagnetic constraints on the structure of the Deccan traps. PEPI 74, 241–261.
Vandamme, D., Courtillot, V., Besse, J., Montigny, R., 1991. Paleomagnetism and age determinations of the Deccan traps (India): results of a Nagpur–Bombay traverse and review of earlier work. Rev. Geophys. 29, 159–190.
Venkatesh, V., 1967. The Lonar crater — some geochemical data. J. Geol. Soc. India 8, 29–37.
Watson, G.S., 1956. A test for randomness of directions. Mon. Not. R. Astron. Soc., Geophys. Suppl. 7, 160–161.
Weiss, B.P., Garrick-Bethell, I., Pederson, S., Louzada, K.L., Stewart, S.T., Maloof, A.C., 2007. Paleomagnetism of impact glass from Lonar crater, India. Lunar and Planetary Science Conference XXXVIII, League City, TX. 2360.
Zijderveld, J.D.A., 1967. A.C. demagnetization of rocks: analysis of rocks. In: Collinson, D.W., Creer, K.M., Runkorn, S.K. (Eds.), Methods in Paleomagnetism. Elsevier, Amsterdam, pp. 254–286.